MM Science Journal | www.mmscience.eu
ISSN 1803-1269 (Print) | ISSN 1805-0476 (On-line)
Special Issue | TEAM 2024
Transdisciplinary and Emerging Approaches to Multidisciplinary Science
11.9.2024 – 13.9.2024, Ostrava, Czech Republic
DOI: 10.17973/MMSJ.2024_10_2024073

TEAM2024-00013

EFFECT OF TECHNOLOGICAL PARAMETERS OF THE PULSATING WATER JET ON EROSION EFFECTIVITY ON A LINEAR TRAJECTORY

J. POLOPRUDSKY[1,2]*, D. KLICHOVA[3] G. STOLARIK[4], A. CHLUPOVA[1]

[1] Institute of Physics of Materials, The Czech Academy of Sciences, Brno, Czech Republic
[2] Institute of Materials Science and Engineering, Brno University of Technology, Czech Republic
[3] Institute of Geonics, The Czech Academy of Sciences, Ostrava-Poruba, Czech Republic
[4] Faculty of Manufacturing Technologies TUKE with a seat in Presov, Slovak Republic

*Corresponding author; e-mail: poloprudsky@ipm.cz

Abstract:

The article focuses on easily adjustable technological parameters controlling the effectiveness of pulsating water jet (PWJ). The first technological parameter is standoff distance; this parameter controls water cluster development and should be set optimal according to process hydraulic parameters. The second parameter is feedrate, this parameter, when considering linear trajectory, controls the impact distribution on the treated area. Four hydraulic pressure levels (30, 40, 50, and 60 MPa) were selected for the experiment. The standoff distance was during the experimental runs ranging from 26 to 68 mm with the goal of finding optimal value. The optimal standoff distance was selected based on Rz and Rv parameters. Rz and Rv values show increasing tendency with increment of standoff distance followed by culmination and then decreasing tendency. The impact distribution ranged from 8 000 to 40 000 impacts per millimeter. The decrease in water impact shows strictly decreasing tendencies in all evaluated parameters. However, the increase in pressure level shows better percentual retainment of erosion effectivity during the lowering of water impact distribution.

Keywords: pulsating water jet, water cluster, droplet, erosion, standoff distance, impact distribution

1 INTRODUCTION

The collision of liquid mass with solid surface creates transient impact pressure p_{wh} that can lead to changes in the surface and subsurface and even to material removal [Adler, 1995]. The impact pressure can be calculated as:

$$p_{WH} = \rho C v_w \quad (1)$$

where ρ is the liquid density, C is the velocity of the compression wave in liquid, and v_w is the velocity of the impacting water element.

This impact pressure acts upon the surface until the release wave generated at the contact edge reaches the edge of the liquid droplet [Hancox and Brunton, 1966].

$$T = \frac{R}{v}\left[1 - \sqrt{\left(1 - \frac{v_w^2}{C^2}\right)}\right] \quad (2)$$

where R is the diameter of the water element. The release of the impact pressure leads to lateral jetting, which can also have a significant damaging effect, especially on surface asperities. The release of the impact pressure leads to a fall of the pressure on the central axis to a level of Bernoulli stagnation pressure p_s [Hancox and Brunton, 1966].

$$p_S = \frac{1}{2}\rho v_w^2 \quad (3)$$

The transient increased impact pressure has been used to significantly increase the effectivity of pure water jet at the same flow conditions [Field, 1999]. In the case of a pure continual water jet (CWJ), the jet acts on the surface under Bernoulli stagnation pressure. However, if the coherent jet is split into separate water bodies (droplets, clusters, elements, etc.), it causes repeated oscillations between impact and stagnation pressures. There are several ways how to divide coherent stream into discrete clusters. The pulsed jets can be created by accelerating the breakage of CWJ or by mechanically splitting the CWJ. The jet separation can be done using an external jet separator such as a rotating disc or mechanical vibrations of the nozzle body. The acceleration of jet breakage can be done by using self-excited oscillations induced by a Helmholtz resonator or fluidic nozzle. The method considered in this work is based on introducing ultrasonically vibrating mechanical elements inside the jet chamber.

This article employs for the formation of a pulsating water jet (PWJ) the ultrasonic modulation created by the vibration of the ultrasonic sonotrode inside the acoustic chamber (see Fig. 1). The device used for this study was developed

by Foldyna [Foldyna and Svehla, 2011] located in the Institute of Geonics, Ostrava. The high-pressure system consists of an integrated acoustic generator, which creates pressure fluctuations inside the acoustic chamber, leading to velocity fluctuations of the jet in the free atmosphere. These fluctuations lead to the shattering of the jet into discrete water clusters.

This methodology of PWJ creation, however, creates numerous technological challenges concerning the tuning of appropriate of several technological parameters, such as standoff distance [Hloch et al., 2019a], hydraulic pressure [Lehocka et al., 2020, Tripathi et al., 2020], frequency [Srivastava et al., 2019], acoustic chamber length [Nag et al., 2019], liquid density [Hloch et al., 2019b], liquid temperature, nozzle geometry, or impact angle, even for the simple case considering stationary processes such as drilling. The individual effect of most of these parameters on erosion effectivity and optimal standoff distance has been extensively studied. For example, the effect of acoustic chamber length on both optimal standoff distance and maximum depth achieved was observed by [Nag et al., 2019] and is attributed to the effectiveness of ultrasonic energy transmission [Nag et al., 2021]. However, a study determining cross-correlation between these individual parameters has not yet been published concerning this type of device.

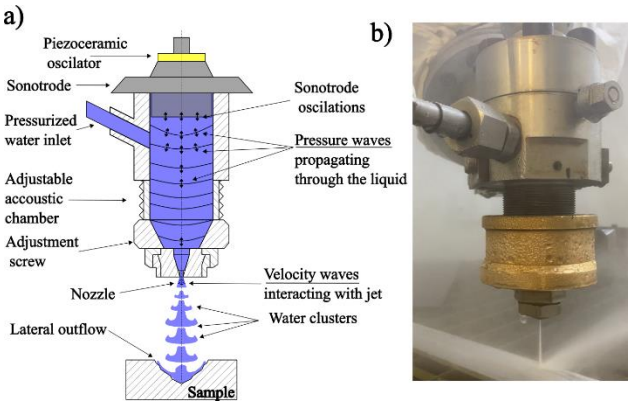

Figure 1 Schematic of the water jet with an acoustic generator of pressure pulsations and adjustable acoustic chamber b) photo of PWJ moving over a sample

The effect of hydraulic pressure on standoff distance was the work focus in [Chlupová et al., 2023, Hloch et al., 2019a, Srivastava et al., 2020]. It was proved by theoretical description and observed using a high-speed visualization [Zelenak et al., 2015] that the standoff distance determines water cluster development (see **Fig.1**). Hloch et al. [Hloch et al., 2020] described five regimes of erosion based on standoff distance.

The lowest range of standoff distance is related to the incubation regime, where the liquid column of PWJ acts in a similar manner to CWJ. The discrete clusters are not yet formed, and stagnation pressure prevails over impact pressure. Nevertheless, it is essential to distinguish between the incubation regime denoted by the standoff distance [Hloch et al., 2020] and the incubation stage, denoted by exposure [Thomas and Brunton, 1970].

The acceleration regime belongs to higher standoff distances than the incubation regime, and it is defined by the acceleration of the erosion rate. In this regime, impact pressure starts to prevail over stagnation pressure, and the formation of the water clusters takes place.

Further increase of standoff distance leads to a state when the erosion rate reaches maximal value. The jet morphology consists of discrete clusters. Each of the water clusters causes impact pressure upon the surface.

The higher range of standoff distance leads to a detrimental effect on erosion rate because exposure of the water clusters to atmospheric drag leads to deconcentration of the radial wave and breakup of discrete clusters into monodisperse droplets [Hloch et al., 2020]. Therefore, the optimal standoff distance lies in the culmination regime where the clusters are discreet and sufficiently developed, which leads to the highest erosion efficiency for given parameters. The optimal standoff distance evaluated by several studies based on hydraulic pressure and nozzle diameter is given in Tab. 1.

Table 1 Optimal standoff distance based on hydraulic pressure evaluated in other studies

Optimal standoff distance	Hydraulic Pressure	Nozzle diameter	Source
mm	MPa	mm	-
45, 70, 100	20, 40, 60	1.9	[Srivastava et al., 2018]
35	40	0.6	[Chlupová et al., 2023]
65, 65, 65, 105	20, 40, 70, 100	1.32	[Klichova et al., 2023]
45	50	0.4	[Poloprudský et al., 2024]

Srivastava et al. [Srivastava et al., 2020] examined differences between the inclined and step trajectories. Step trajectory is based on running at a constant standoff distance for a given length, then increasing the standoff distance, and then another run at a new constant value of standoff distance. The inclined trajectory is determined by a jet movement at a certain angle to the surface. The inclined trajectory doesn't consider the vertical velocity component :

$$v_y = v.\sin\alpha \tag{4}$$

where *v* is feedrate, α is the angle of PWJ trajectory and v_y is the vertical component of PWJ device trajectory This component decreases the impact force because it creates a decrement in jet velocity:

$$v_w = v_{PWJ} - v_y \tag{5}$$

where v_{PWJ} is the velocity of water clusters generated by PWJ. Based on the results proposed by [Srivastava et al., 2020], the step trajectory is more advantageous because it achieves higher erosion depth. Moreover, the inclined trajectory may have a detrimental effect on the results and optimal standoff distance evaluation. It is the reason why a stair trajectory is now generally prefered and is employed in this work. The second reason for choosing the stair trajectory was to avoid the possible doppler effect, as suggested by [Hloch et al., 2022]

This paper deals with tests of the erosion effectivity of 4 selected hydraulic pressure levels at variable standoff distances, evaluated based on roughness measurement and SEM observation. The goal is to determine the optimal standoff distance from the point of view of the erosion rate for each pressure level.

Under the assumption that at the optimal standoff, the jet produces discrete water clusters at a rate of frequency equal to the frequency of the sonotrode, the feedrate of the jet apparatus can be recalculated into the number of impacts on mm by the following equation:

$$I_d = \frac{f}{v} \quad (6)$$

where I_d is the cluster distribution, *f* is the frequency of the sonotrode, and *v* is the velocity of the PWJ apparatus movement on a linear trajectory (feedrate).

The effect of the number of impacts per mm will be evaluated in this work to create a necessary link between static exposure where the PWJ apparatus is stationary over the surface, such as in erosion tests [Nag et al., 2024], erosion prediction [Poloprudský et al., 2024], drilling and dynamic exposure processes such as cutting [Raj et al., 2020], surface peening [Siahpour et al., 2023] or surface roughening [Klichova et al., 2023].

2 MATERIALS AND METHODS

2.1 Material

Austenitic stainless steel AISI316L for the experiment was supplied as a hot rolled plate. The selected material shows great structural homogeneity with only a small amount of residual δ ferrite in the form of elongated bands located primarily in the middle of the plate in the rolling direction.

The grain size of the material was evaluated using electron back-scattered diffraction with over 95% hit rate. The arithmetic mean grain size measured as equivalent circle diameter is 10±7 μm without joining special/twin boundaries and 16±12 μm with the joining of special/twin boundaries. The area-weighted mean equivalent circle diameters evaluated from the EBSD map are 19 μm and 32 μm without and with the joining of special/twin boundaries. Hardness was evaluated using a Duramin microhardness tester (Struers, Denmark) with a load of 1.96 N from five measurements as184±10 HV0.2.

Samples for PWJ treatment were prepared by mechanical grinding with abrasive paper of average grain sizes of 46 μm, 22 μm, 18 μm, and 15 μm, followed by polishing using diamond paste with a grain size of 3 μm. Both grinding and polishing were done on ATM Saphir 320 and Saphir 330 (ATM Qness, Germany).

2.2 Experiment

Experimental runs at four hydraulic pressure levels, 30, 40, 50, and 60 MPa, were conducted using PWJ technology stationed in the Institute of Geonics, The Czech Academy of Sciences in Ostrava. The maximal pressure level was selected to achieve subsonic flow speed. Selection of lower pressure levels leads to lower water expenditure per unit of time. Pressure levels were selected based on the frequency and mechanical properties of the material to achieve surface roughening and initiation of material removal within the selected impact distribution. The PWJ head was moving parallel to the surface with an increase in standoff distance between each measured trajectory. This approach is a variation of stair trajectory (Fig. 2). The difference is that the vertical step is done outside the sample, and the vertical steps are not equidistant but designed for the fastest determination of optimal standoff distance.

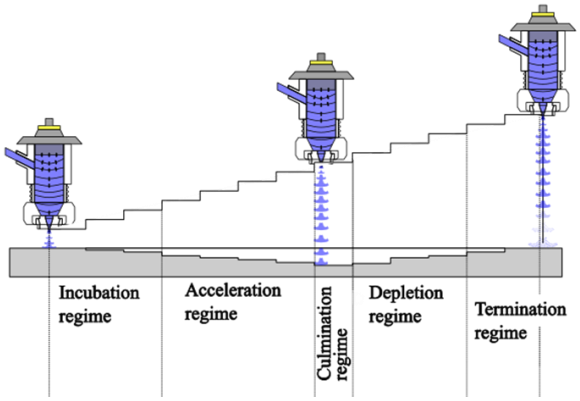

Figure 2 Stair trajectory of PWJ head devised to evaluate optimal standoff distance for hydraulic conditions based on [Hloch et al., 2020, Srivastava et al., 2020]

The technological conditions of the experiment are listed in Tab. 2. The *p* stands for hydraulic pressure, f_s for starting frequency, and l_c for acoustic chamber length. Optimal l_c was selected based on the methodology proposed by [Nag et al., 2021]. A nozzle with a diameter of 0.5 mm was constant for all tests. For each pressure level, the only variable is a standoff distance varied within the range specified in Tab. 2. Fig. 3 shows a graph of the tested standoff distances for each pressure level, with highlighted standoff distances selected as optimal based on Rz and Rv values presented in Chapter 3: results.

Table 2 Experiment concerning variable impact development controlled by standoff distance for each hydraulic pressure level.

Exp No.	p	f_s	l_c	Flow speed	Flow rate	Standoff distance variation
	MPa	*kHz*	*mm*	*m/s*	*l/min*	*mm*
1	30	40.7	8	220.7	2.6	26-32
2	40	40.5	10	254.8	3.0	26-38
3	50	40.4	11	284.9	3.4	30-46
4	60	40.7	11	312.1	3.7	40-68

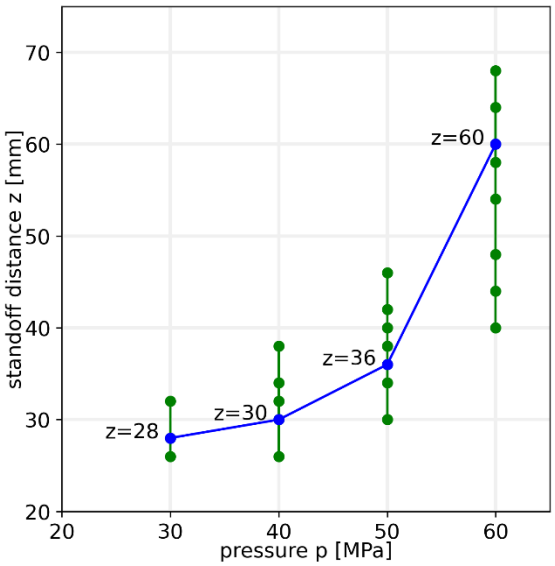

Figure 3 Graphical visualization of standoff distance variation used for the experiment with highlighted selected optimal standoff distance

These optimal standoff distances were determined and listed in Tab. 3**,** together with the impact distribution controlled by the federate. Feedrate set to a value of 1;5 mm/s resulted in an impact distribution of 40 000 and 8 000 imp/mm for lower pressure levels (30 and 40 MPa) and federate of 1; 5; 10 mm/s resulted in an impact distribution of 40 000, 8 000 and 4 000 imp/mm for higher pressure levels (50 and 60 MPa) (see **Fig. 4**). The top part of the figure shows the side view, while the bottom part shows the top view.

Table 3 Experiment concerning variable impact distribution controlled by feedrate for each hydraulic pressure level.

Exp No.	p	f_s	l_c	Flow speed	Flow rate	**Optimal standoff**	Feed rate	Impact distribution
	MPa	*kHz*	*mm*	*m/s*	*l/min*	***mm***	*mm/s*	*imp/mm*
1	30	40.7	8	220.7	2.6	**28**	1-5	40 000-8 000
2	40	40.5	10	254.8	3.0	**30**	1-5	40 000-8 000
3	50	40.4	11	284.9	3.4	**36**	1-10	40 000-4 000
4	60	40.7	11	312.1	3.7	**60**	1-10	40 000-4 000

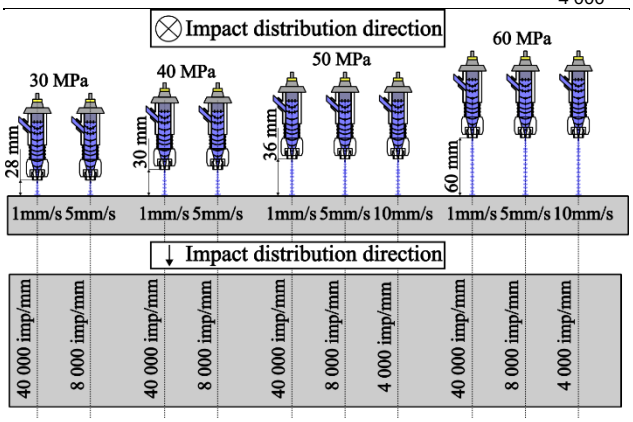

Figure 4 Experimental parameters and design for evaluation of the effect of water impact distribution controlled by feedrate

2.3 Measurements

The decisive roughness parameters for the treated surface were evaluated using a laser confocal microscope OLYMPUS LEXT OLS 3100. The characterization consisted of assessing the roughness parameters according to ISO 21920-2. The settings for the evaluation of the selected profile roughness parameters were made according to ISO 21920-3. The Gaussian filter was according to ISO 16610-21. The nesting index of profile L-filter = 0.8 mm was selected for roughness evaluation. The cut-off frequency divides the assessment length into several sampling lengths from which roughness parameters are evaluated as described in ISO 21920-3. The evaluated line length was set to 4.0 mm. The evaluation consisted of Ra (arithmetic mean height), Rz (maximum height), and Rv (mean pit depth) determination.

Surface observation to evaluate the erosion mechanism and erosion level was done using a scanning electron microscope (SEM) Tescan Lyra 3 XMH FEG/SEMxFIB (Tescan, Czech Republic) equipped with EBSD detector Symmetry operated by Aztec software (Oxford Instruments, United Kingdom) used for grain size analysis.

3 RESULTS

The effect of PWJ parametric variation on the surface of austenitic stainless steel AISI 316L was evaluated. The progress of roughness parameters based on the standoff distance of 4 different pressure levels was evaluated at a constant feedrate of 1 mm/s (see Fig. 5) . The dependence of Ra on standoff distance is most notable for a pressure level of 30 MPa; in the case of higher pressure levels, the dependence is much less apparent. The hydraulic pressure of 30 MPa achieves surface roughness Ra in the range from 1.48 µm up to 1.84 µm in a standoff distance range of 26 to 32. The hydraulic pressure of 40 MPa led to a roughness range from 2.32 µm to 2.77 µm in a standoff distance range of 26 to 38 mm. The pressure of 50 MPa created profile roughness Ra ranging from 2.36 µm up to 2.74 µm for standoff distance intervals from 30 to 46 mm. The highest hydraulic pressure level of 60 MPa caused Ra roughness to range from 2.27 µm to 2.81 µm for a standoff distance range of 40 to 68 mm.

The highest Ra value based on standoff distance in almost all hydraulic pressures coincides with the highest Rz parameter. The exception is observed at the pressure level of 50 MPa, where the highest Rz parameter was observed at a standoff distance of 36 mm, while the highest Ra value was observed at a standoff distance of 38 mm.

Rz and Rv roughness parameters show the trend caused by standoff distance variation. From the comparison of the results in Fig. 5, it appears the Rv parameter describes changes due to cluster development most readily.

The maximum values for Rz achieved at each pressure level reached Rz 13.64 µm at standoff distance of 28 mm for hydraulic pressure of 30 MPa, Rz 20.65 µm at standoff distance of 30 mm for hydraulic pressure of 40 MPa, Rz 21.48 µm at standoff distance of 36 mm for hydraulic pressure of 50 MPa and finally Rz 21.98 µm at standoff distance of 54 mm for hydraulic pressure of 60 MPa. Exposure of the surface to PWJ at a hydraulic pressure of 60 Mpa causes almost linear growth of the Rv parameter in standoff distance range from 40 mm to 58 mm. It can be concluded that both Rz and Rv parameters show growing and decreasing tendencies, pointing to the existence of optimal standoff distance. Based on these results, optimal standoff distances were selected and highlighted in **Fig. 3**. The standoff distances selected as optimal are 28, 30 , 36, and 60 mm for hydraulic pressure levels 30, 40, 50, and 60 MPa, respectively.

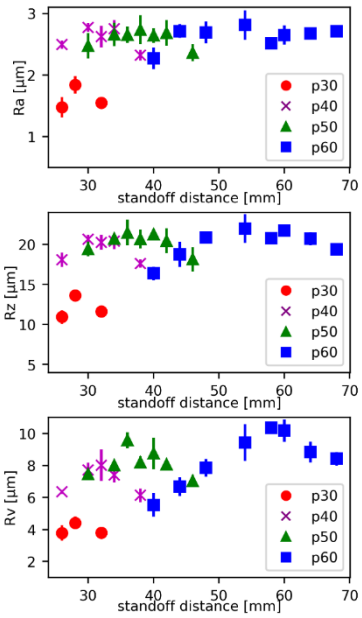

Figure 5 Roughness parameters Ra, Rz, Rv of 4 pressure levels based on standoff distance

The surface of the austenitic steel samples was then exposed to PWJ treatment at these optimal standoff distances at each pressure level with variable feedrate. An increase in feedrate caused a controlled decrease in the total number of cluster impacts by decreasing the water cluster impacts per millimeter (imp/mm). The feedrate values selected were 1 and 5 mm/s for two lower hydraulic pressure levels, creating an impact distribution of 40 000 imp/mm and 8 000 imp/mm. On the other hand, for higher hydraulic pressure levels, feedrate values tested were 1, 5, and 10 mm/s, leading to cluster impact distribution of 40 000, 8 000, and 4 000 imp/mm, respectively. The surface roughness profile evaluation in Fig. 6 shows the effect of impact distribution on one of the roughness parameters (Ra, Rz, Rv) for each of the four examined hydraulic pressure levels. All of the roughness parameters show a strictly decreasing tendency. A decrease of cluster impact distribution from 40 000 to 8 000 imp/mm (20%) leads to a lowering of Rz to 60.7 % caused by 40 000 imp/mm at the highest hydraulic pressure level of 60 MPa. With the decrease in hydraulic pressure, this percentage also decreases, and at a hydraulic pressure of 30 MPa, it reaches 39.1 %. A similar effect is observed when changing cluster impact distribution from 40 000 to 4 000 imp/mm (10 %), which leads in the case of hydraulic pressure 60 MPa to achieving 40.5 % of the Rz value caused by 40 000 imp/mm, while in the case of hydraulic pressure 50 MPa it is 37.6 %.

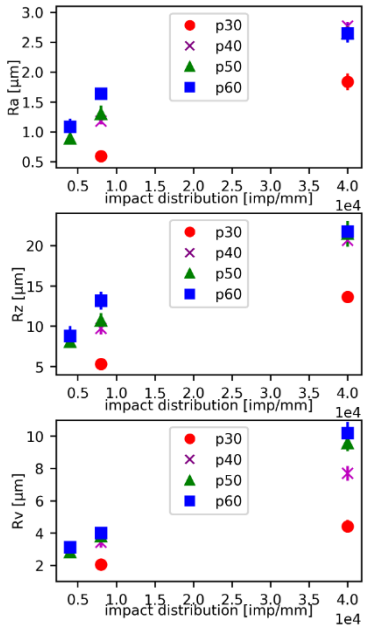

Figure 6 Roughness parameters Ra, Rz, Rv of 4 pressure levels based on impact distributions at optimal standoff distances z_{opt} selected for each pressure level p = 30, 40, 50, 60 MPa as 28, 30, 36, 60 mm respectively

Fig. 7 shows a compilation of SEM micrographs. showing surfaces treated at optimal standoff distances for each hydraulic pressure level and two water impact distribution levels 40 000 and 8 000 imp/mm. The pressure variation at the impact distribution of 40 000 imp/s leads to material roughening. There are observable places with significant localized material removal. This localized material removal was observed very sporadically at a hydraulic pressure of 40 MPa. With higher pressure levels of 50 MPa and 60 MPa, the number of areas with signs of material removal and surface defects increases. The impact distribution of 8 000 imp/mm led to surface roughening without visible material removal for observed pressure levels.

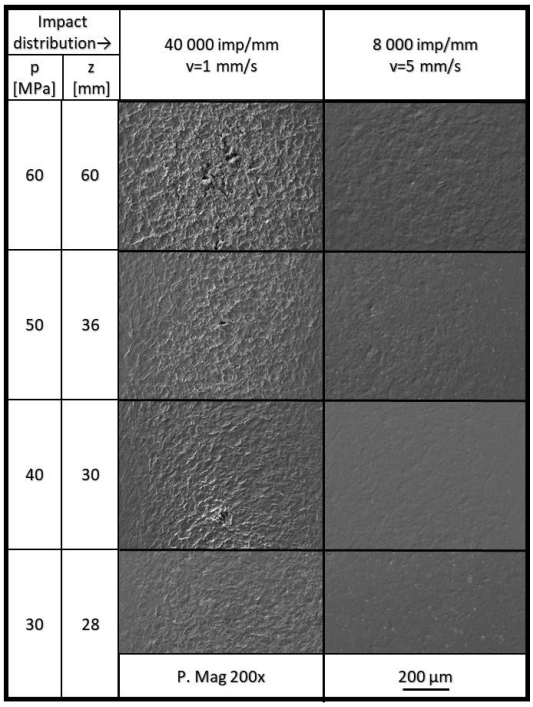

Figure 7 SEM overview of parametric optimization for the 316L steel considering pressure p standoff distance z and feed rate v with SEM print magnification of 200x

Fig. 8 shows a detailed observation of erosion processes for each pressure level and two impact distributions. The lower pressure levels show the creation of surface steps inside individual grains and the exposition of grain boundaries. The highest hydraulic pressure level leads to connected cavities upon the observed surface. The impact distribution 8 000 imp/mm leads to surface roughening without observed material removal. The most notable observable surface asperities are steps inside grains, probably caused by deformation twining or the creation of surface steps on the original twins.

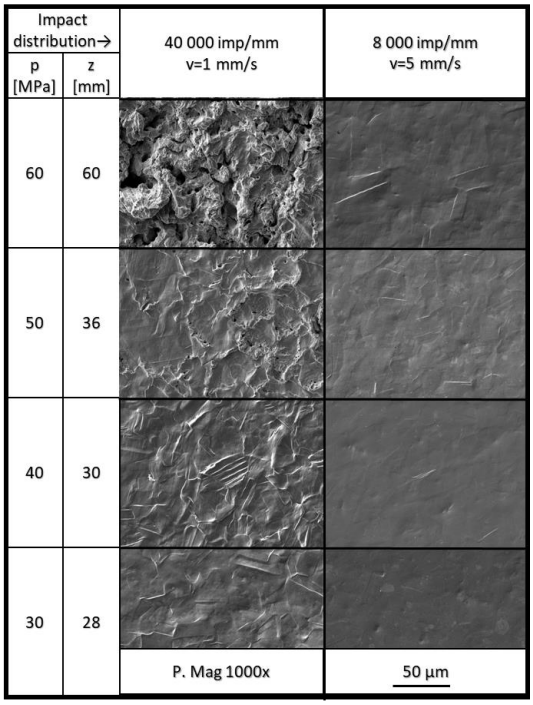

Figure 8 SEM detail of effect of parametric optimization considering pressure P standoff distance z and feed rate v with SEM print magnification of 1000 x

Fig. 9 shows micrographs taken at a print magnification of 100x stitched to cover the whole erosion kerf. The picture shows erosion kerfs created by hydraulic pressure of 50 and 60 MPa. A significant observation is the inconsistency of the kerf width and erosion effectivity across the PWJ jet trajectory.

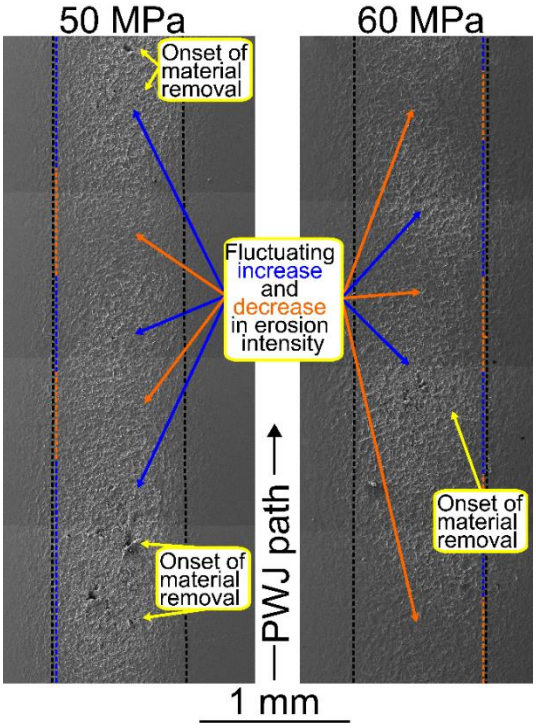

Figure 9 stitched SEM micrographs showing the considerable length of erosion kerfs created at optimal standoff distances at hydraulic pressure levels of 50 and 60 Mpa

4 DISCUSSION

The surface of austenitic steel AISI 316L was treated in ranges of hydraulic pressures from 30 to 60 MPa, standoff distance in a range from 26 to 68 mm, and impact distribution in the range from 40 000 to 8 000 imp/mm.

The chosen parameters created a repeated impact of liquid clusters on the surface of the sample at subsonic speed. SEM observations showed a high number of exposed grain boundaries and, at a high hydraulic pressure level, many surface cavities. In most cases, the depth of the kerf [Chlupová et al., 2023] or volume removed [Foldyna et al., 2009] is used for the evaluation of optimal standoff distance. However, material removal across the whole kerf was not observed at process parameters within the experimental design. Therefore, a different approach was chosen, and Rz was used for optimal standoff distance evaluation. Based on the Rz parameter evolution with changes in standoff distance, the optimal standoff distance evaluated within this experiment should overlap with the culmination regime described by Hloch et al. [Hloch et al., 2020]. The most probable reason why no global material removal occurred is due to material selection and set-up of process parameters. The experimental material is austenitic steel with hardness reaching almost 200 HV0.2, while in other works [Hloch et al., 2019a, Nag et al., 2019] softer aluminum alloy for optimal standoff distance evaluation is used. The selection of soft material increases the response to PWJ process changes. The second reason was that the PWJ process parameters, namely hydraulic pressure, were adopted to create a subsonic flow speed of the jet reaching about 312.1 m/s at the highest hydraulic pressure level. Lastly, surfaces were thoroughly polished before the PWJ exposure by diamond paste with a grain size of 1 μm. The polishing was done to observe better erosion incubation expected at lower impact distribution. However, according to Kirols et al. [Kirols et al., 2015], improvement of the initial surface roughness delays the water impact erosion. Therefore, mechanically or electrochemically polished surfaces may be beneficial for incubation erosion stage observation but may delay the onset of erosion effects.

Experiments show a significant increase in Rz and Rv achieved with an increase in pressure from 30 to 40 MPa. This increment in Rz and Rv achieved is getting less significant with each further increase of hydraulic pressure. There are two possible reasons. First is that sonotrode ability to create discrete clusters is hindered at higher pressure levels. The second reason comes from equations (1) and (3), since higher pressure leads to higher impact speed v_w. As v_w increases closer to the value of C (velocity of a compression wave in liquid), the difference between impact pressure and stagnation pressure decreases.

The surface roughness Ra of this study is comparable to the study [Srivastava et al., 2018]. The roughness of the target material of the AISI304L weld joint was increased with an increase in the operating pressure of 20-60 MPa, which was attributed to the higher kinetic energy of the incident jet. The measured roughnesses at 20, 40, and 60 MPa were Ra= 2.58, 3.47, and 2.86 μm compared to 2.77 and 2.81 μm at 40 and 60 MPa in this study. Surface roughness deviations can be attributed to the larger diameter of the nozzle d = 1.9 mm, which also caused higher standoff distances of 45, 70, and 100 mm for the pressures used. This trend can also be confirmed in comparison with [Srivastava et al., 2021]. In this case, a pressure of 40 MPa and a nozzle diameter of 1.9 mm caused a roughness of 6.08 μm and 4.26 μm at frequencies of 40 and 20 kHz. These roughnesses are on the order of two to three times higher compared to the presented study. This can be attributed to the nearly 3-fold enlargement of the nozzle. It can be seen that the technological parameters of the PWJ method are sensitive to the volume of water flowing through the nozzle, which also causes a different effect on the target surface. The same material was also used in [Srivastava et al., 2022] using pressures of 40, 60, and 80 MPa and a nozzle diameter of 1.19 mm. The results show that the parameter Ra decreases from 1.4 to 0.8 μm with an increase in pressure of 40-80 MPa. The reduction in roughness was attributed to preventing the movement of the sonotrode as the pressure increased, resulting in a reduction in the generation of fluctuating pressure and, thus, water clusters. However, these results were realized at the same standoff distance, z= 31 mm, without its optimal tuning. In this case, the technology was not tuned to its optimal parameters, and this resulted in a reduction of its erosion potential. Therefore, it can be concluded that without tuning the optimal distance parameter, it is not possible to compare erosion between different technological parameters in a relevant way.

The other explanation may be that insufficient formation of water clusters occurs at high pressure levels and lower standoff distances. Measured data show that optimal standoff distance increases with increasing hydraulic pressure level. It was observed [Zelenak et al., 2015] that too high standoff distance can cause the deconcentration of water clusters due to atmospheric drag.

The effect of impact distribution has also been observed, and these early results suggest that higher hydraulic

pressure leads to a lower Rz-parameter decrease due to a reduction in impact distribution.

Feedrate was selected as a parameter for controlling impact distribution. Concerning PWJ moving on a linear trajectory, controlling impact distribution is the most applicable parameter. In the case of stationary PWJ exposition, exposure time plays a similar role. In the case of 2D surface treatment combination of feedrate and overlapping factor play a similar role. Another parameter for changing impact distribution in the case of linear trajectory would be (according to equation 6) a change of frequency. However, a significant change of frequency would, in the current setup, require changing of sonotrode, which is, from a technological point of view, a considerably more complex task than a change of feedrate. The second problem is that a change in frequency would also lead to a change in the volume of impacting water mass, which has to be taken into consideration.

The inhomogeneity of the jet path across longer trajectories, seen in Fig. 9, can be attributed to several factors. Future tests should aim to elucidate this behavior. It was described in the introduction, according to [Hloch et al., 2020] that at higher standoff distances, the water cluster is deconcentrated due to atmospheric drag. The erosion effectivity of PWJ is very sensitive to standoff distance. Furthermore, [Stolárik et al., 2023] described that the actual generated frequency of the sonotrode is dependent on the resistance of the sonotrode. This means the frequency can deviate during the experiment from the starting frequency. The deviations in the frequency affect the volume of water clusters and their resistance to air drag, leading to changes in erosion effectiveness. Testing this theory would require monitoring the current frequency during the experiment.

The study focuses on tunning the effect of PWJ technology on the surface of AISI 316L via water cluster development and water impact distribution controlled via technologically easily adjustable parameters standoff distance and feedrate, respectively. The results of this study could be used for the optimization of surface roughening of AISI316L and transferred to a group of austenitic steels with similar mechanical and structural properties. Austenitic stainless steels are often used as biomaterials where a controlled increase of roughness could promote cell growth [Gentile et al., 2010].

The future scope of research will be focused on additional process and hydraulic parameters and creating correlations between them for a more comprehensive understanding and usability of the technology. Parameters of immediate interest include the geometry of the nozzle, as it is easily adjustable and influences water cluster volume. Our study was focused on the perpendicular impact of PWJ clusters on the sample surface. Nevertheless, the angle of impingement is a very critical parameter both from erosion prediction and treatment of complex surfaces point of view and will be focused on in future studies. Water temperature influences water viscosity and is an important variable when simulating natural erosion conditions. The final goal is to create a cross-correlation table between the tested parameters.

5 SUMMARY

An experimental setup consisting of linear trajectories was applied. The first set of experiments had set hydraulic parameters at four hydraulic pressure levels, 30, 40, 50, and 60 MPa, and variance in water cluster development was controlled via standoff distance setting. The result of the experimental campaign was to evaluate the optimal standoff distance for each hydraulic pressure level. The second set of experiments used optimal standoff distances and varied water impact distribution controlled via feedrate. The following conclusions can be made:

- Rz and Rv value shows dependence on standoff distance for all pressure levels with an increasing tendency up to culmination and then a decreasing tendency.
- Based on the Rz and Rv trend, the optimal standoff distance can be evaluated for harder materials that do not exhibit erosion material removal stage under given hydraulic/technological conditions.
- The decrease in water impact distribution shows strictly decreasing tendencies in the case of Ra, Rz, and Rv parameters.
- The increase in pressure level shows better percentual retainment of erosion effectivity during water impact distribution decrease.
- Surface roughening is, in the initial stages, driven by exposing the grain boundaries.

6 ACKNOWLEDGMENTS

The financial support received from the Czech Science Foundation, project GAČR 23–05372S, is gratefully acknowledged. The PWJ treatment was carried out at the Institute of Geonics, The Czech Academy of Sciences.

7 REFERENCES

[Adler, 1995] Adler, W. F.: 'Waterdrop impact modeling'; Wear, 186–187 (1995), 341–351. https://doi.org/10.1016/0043-1648(95)07176-8

[Chlupová et al., 2023] Chlupová, A., Hloch, S., Nag, A., Šulák, I., Kruml, T.: 'Effect of pulsating water jet processing on erosion grooves and microstructure in the subsurface layer of 25CrMo4 (EA4T) steel'; Wear, 524–525 (2023), 204774. https://doi.org/10.1016/j.wear.2023.204774

[Field, 1999] Field, J. E.: 'ELSI conference: invited lecture'; Wear, 233–235 (1999), 1–12. https://doi.org/10.1016/S0043-1648(99)00189-1

[Foldyna et al., 2009] Foldyna, J., Sitek, L., Ščučka, J., Martinec, P., Valíček, J., Páleníková, K.: 'Effects of pulsating water jet impact on aluminium surface'; Journal of Materials Processing Technology, 209, 20 (2009), 6174–6180. https://doi.org/10.1016/j.jmatprotec.2009.06.004

[Foldyna and Svehla, 2011] Foldyna, J., Svehla, B.: 'Method of Generation of Pressure Pulsations and Apparatus for Implementation of this Method'; The Journal of the Acoustical Society of America, 129, 2 (2011), 1133. https://doi.org/10.1121/1.3561519

[Gentile et al., 2010] Gentile, F., Tirinato, L., Battista, E., Causa, F., Liberale, C., Di Fabrizio, E. M., Decuzzi, P.: 'Cells preferentially grow on rough substrates'; Biomaterials, 31, 28 (2010), 7205–7212. https://doi.org/10.1016/j.biomaterials.2010.06.016

[Hancox and Brunton, 1966] Hancox, N. L., Brunton, J. H.: 'The Erosion of Solids by the Repeated Impact of Liquid Drops'; Philosophical Transactions of the Royal Society of London. Series A, Mathematical and Physical Sciences, 260, 1110, (1966), 121–139.

[Hloch et al., 2019a] Hloch, S., Adamčík, P., Nag, A., Srivastava, M., Čuha, D., Müller, M., et al.: 'Hydrodynamic ductile erosion of aluminium by a pulsed water jet moving

in an inclined trajectory'; Wear, 428–429 (2019a), 178–192. https://doi.org/10.1016/j.wear.2019.03.015

[Hloch et al., 2019b] Hloch, S., Nag, A., Pude, F., Foldyna, J., Zeleňák, M.: 'On-line measurement and monitoring of pulsating saline and water jet disintegration of bone cement with frequency 20 kHz'; Measurement, 147 (2019b), 106828. https://doi.org/10.1016/j.measurement.2019.07.056

[Hloch et al., 2022] Hloch, S., Sousek, K., Svobodova, J., Hromasová, M., Müller, M.: 'Subsurface microtunneling in ductile material caused by multiple droplet impingement at subsonic speeds'; Wear, 490–491 (2022), 204176. https://doi.org/10.1016/j.wear.2021.204176

[Hloch et al., 2020] Hloch, S., Srivastava, M., Nag, A., Müller, M., Hromasová, M., Svobodova, J., et al.: 'Effect of pressure of pulsating water jet moving along stair trajectory on erosion depth, surface morphology and microhardness'; Wear, 452–453 (2020), 203278. https://doi.org/10.1016/j.wear.2020.203278

[Kirols et al., 2015] Kirols, H. S., Kevorkov, D., Uihlein, A., Medraj, M.: 'The effect of initial surface roughness on water droplet erosion behaviour'; Wear, 342–343 (2015), 198–209. https://doi.org/10.1016/j.wear.2015.08.019

[Klichova et al., 2023] Klichova, D., Nag, A., Poloprudsky, J., Foldyna, J., Pude, F., Sitek, L., Hloch, S.: 'Utilising of water hammer effect for surface roughening of Ti6Al4V'; The International Journal of Advanced Manufacturing Technology, 126, 11–12 (2023), 5633–5647. https://doi.org/10.1007/s00170-023-11521-y

[Lehocka et al., 2020] Lehocka, D., Botko, F., Klich, J., Sitek, L., Hvizdos, P., Fides, M., Cep, R.: 'Effect of pulsating water jet disintegration on hardness and elasticity modulus of austenitic stainless steel AISI 304L'; The International Journal of Advanced Manufacturing Technology, 107, 5–6 (2020), 2719–2730. https://doi.org/10.1007/s00170-020-05191-3

[Nag et al., 2024] Nag, A., Gupta, M., Ross, N. S., Klichova, D., Petrů, J., Krolczyk, G. M., Hloch, S.: 'Real-time prediction and classification of erosion crater characteristics in pulsating water jet machining of different materials with machine learning models'; Archives of Civil and Mechanical Engineering, 24, 2 (2024), 97. https://doi.org/10.1007/s43452-024-00908-7

[Nag et al., 2019] Nag, A., Hloch, S., Cuha, D., Dixit, A. R., Tozan, H., Petrů, J., et al.: 'Acoustic chamber length performance analysis in ultrasonic pulsating water jet erosion of ductile material'; Journal of Manufacturing Processes, 47 (2019), 347–356. https://doi.org/10.1016/j.jmapro.2019.10.008

[Nag et al., 2021] Nag, A., Stolarik, G., Svehla, B., Hloch, S.: 'Effect of Water Flow Rate on Operating Frequency and Power During Acoustic Chamber Tuning'; In S. Hloch, D. Klichová, F. Pude, G. M. Krolczyk & S. Chattopadhyaya (Eds.), Advances in Manufacturing Engineering and Materials II. Cham: Springer International Publishing (2021), 142–154. https://doi.org/10.1007/978-3-030-71956-2_13

[Poloprudsky et al., 2024] Poloprudský, J., Gamanov, S., Chlupova, A., Klichova, D., Nag, A., Stolarik, G., Hloch, S.: 'Water droplet erosion assessment in the initial stages on AISI 316 L using kernel average misorientation'; Tribology International, 191 (2024), 109165. https://doi.org/10.1016/j.triboint.2023.109165

[Raj et al., 2020] Raj, P., Chattopadhyaya, S., Mondal, A.: 'A review on continuous and pulsed water jet machining'; Materials Today: Proceedings, 27 (2020), 2596–2604. https://doi.org/10.1016/j.matpr.2019.11.071

[Siahpour et al., 2023] Siahpour, P., Amegadzie, M. Y., Tieu, A., Donaldson, I. W., Plucknett, K. P.: 'Ultrasonic pulsed waterjet peening of commercially-pure titanium'; Surface and Coatings Technology, 472 (2023), 129953. https://doi.org/10.1016/j.surfcoat.2023.129953

[Srivastava et al., 2018] Srivastava, M., Hloch, S., Krejci, L., Chattopadhyaya, S., Dixit, A. R., Foldyna, J.: 'Residual stress and surface properties of stainless steel welded joints induced by ultrasonic pulsed water jet peening'; Measurement, 127 (2018), 453–462. https://doi.org/10.1016/j.measurement.2018.06.012

[Srivastava et al., 2022] Srivastava, M., Hloch, S., Krejci, L., Chattopadhyaya, S., Gubeljak, N., Milkovic, M.: 'Utilizing the water hammer effect to enhance the mechanical properties of AISI 304 welded joints'; The International Journal of Advanced Manufacturing Technology, 119, 3–4 (2022), 2317–2328. https://doi.org/10.1007/s00170-021-08357-9

[Srivastava et al., 2019] Srivastava, M., Hloch, S., Muller, M., Hromasová, M., Cais, J., Chattopadhyaya, S., et al.: 'Effect of Frequency Change During Pulsed Waterjet Interaction with Stainless Steel'; In S. Hloch, D. Klichová, G. M. Krolczyk, S. Chattopadhyaya & L. Ruppenthalová (Eds.), Advances in Manufacturing Engineering and Materials. Cham: Springer International Publishing (2019), 85–96. https://doi.org/10.1007/978-3-319-99353-9_10

[Srivastava et al., 2020] Srivastava, M., Nag, A., Chattopadhyaya, S., Hloch, S.: 'Standoff Distance in Ultrasonic Pulsating Water Jet'; Materials, 14, 1 (2020), 88. https://doi.org/10.3390/ma14010088

[Srivastava et al., 2021] Srivastava, M., Nag, A., Krejčí, L., Petrů, J., Chattopadhyaya, S., Hloch, S.: 'Effect of Periodic Water Clusters on AISI 304 Welded Surfaces'; Materials, 14, 1 (2021), 210. https://doi.org/10.3390/ma14010210

[Stolarik et al., 2023] Stolarik, G., Klichová, D., Poloprudsky, J., Nag, A., Hloch, S.: 'Assessment of surface irregularities created by controlled liquid droplet on the surface of stainless steel AISI 304L'; Engineering Science and Technology, an International Journal, 47 (2023), 101558. https://doi.org/10.1016/j.jestch.2023.101558

[Thomas and Brunton, 1970] Thomas, G. P., Brunton, J. H.: 'Drop impingement erosion of metals'; Proceedings of the Royal Society of London. A. Mathematical and Physical Sciences, 314, 1519 (1970), 549–565. https://doi.org/10.1098/rspa.1970.0022

[Tripathi et al., 2020] Tripathi, R., Hloch, S., Chattopadhyaya, S., Klichová, D., Scucka, J., Das, A. K.: 'Application of the pulsating and continous water jet for granite erosion'; International Journal of Rock Mechanics and Mining Sciences, 126 (2020), 104209. https://doi.org/10.1016/j.ijrmms.2020.104209

[Zelenak et al., 2015] Zelenak, M., Foldyna, J., Scucka, J., Hloch, S., Riha, Z.: 'Visualisation and measurement of high-speed pulsating and continuous water jets'; Measurement, 72 (2015), 1–8. https://doi.org/10.1016/j.measurement.2015.04.022